A CBPWM Strategy with Flexible Zero-Sequence Voltage Injection for Three-Level TNPC Converters in Aircraft Electric Starter/Generator System

Feng Guo, Yue Zhao
Power Electronic Systems Laboratory at Arkansas (PESLA)
University of Arkansas
Fayetteville, AR, 72701, United States
fengg@uark.edu, yuezhao@uark.edu

Patrick Wheeler
Power Electronics, Machines and Control (PEMC) Group
University of Nottingham
Nottingham, NG7 2RD, United Kingdom
pat.wheeler@nottingham.ac.uk

***Abstract*—In this paper, a flexible zero-sequence voltage (ZSV) injection method is presented for the silicon carbide (SiC)-based three-level electric starter/generator (ESG) system. The proposed algorithm can automatically adapt based on the operating conditions of the studied ESG system, thus not only capacitor voltages are kept balanced, but also the switching loss is reduced over a wide-speed range operation. Moreover, the abrupt commutation phenomenon that is a common issue for the state-of-the-art discontinuous pulse-width-modulation (DPWM) scheme operating in a low modulation index, is effectively avoided. The results of the simulation and experimental test validate the effectiveness and significant improvement of the introduced modulation technique for a next-generation high power-density aircraft three-level power generation unit.**

***Index Terms*—More-electric-aircraft (MEA), neutral-point voltage balance, switching loss, three-level, zero-sequence voltage**

I. Introduction

The more-electric-aircraft (MEA), aiming at substituting pneumatic, hydraulic and mechanical power by electrical counterparts, has become the state-of-art in aerospace applications over the last few decades [1]. One of the key concepts of the MEA is the electric starter/generator (ESG) system, as illustrated in Fig.1. In comparison with the existing multilevel power electronics building block (PEBB), such as cascaded H-bridge (CHB) [2]-[4], super-cascode power switch [5] and multi-port converter [6]-[9], the three-level T-type neutral-point-clamped (3L-TNPC) converter shown in Fig.2 is chosen as the candidate to manufacture as a result of the reduced electromagnetic interference (EMI), lower harmonic and the minimum switch count [8]. With the help of the wide-bandgap (WBG) technologies [9], [10], the silicon-carbide (SiC) power module is used for building the T-type three-level converter for the purpose of high efficiency and high power-density.

In terms of the configuration of the studied system, a permanent magnet synchronous motor (PMSM) is mechanically connected with aircraft engine shaft and is electrically connected with the converter. In the initial stage of operation, the converter runs as an inverter, which drives the PMSM to crank engine compressor. When the machine speed approaches 10 krpm, the main engine ignites. The generation mode starts once the machine speed approaches 20 krpm during the cruise. In this mode, the engine cranks the machine that works as a generator and the 3L-TNPC converter serves as a rectifier that converts the electrical power from variable-frequency ac to dc for supplying the onboard loads. An overall control block diagram for the studied ESG system is shown in Fig.3.

This work was supported by in part by the U.S. National Science Foundation (NSF) Center on Grid Connected Advanced Power Electronic Systems (GRAPES) under Grant 1939144.

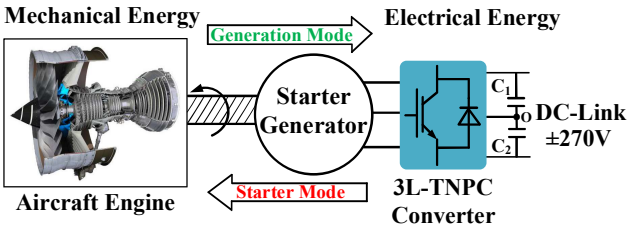

Fig. 1: Aircraft ESG system structure.

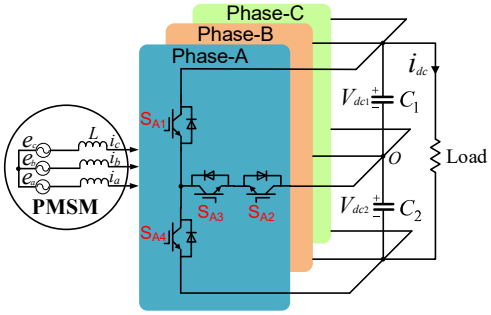

Fig. 2: Topology of 3L-TNPC converter-fed PMSM drives.

However, one of the inherent challenges for the family of NPC topology is the neutral-point (NP) voltage drift issue. The disadvantages render extra over-stress on power devices and induce low-order harmonics in the ac side. To address this problem, two types of modulation algorithms become mainstream. The former is the space-vector PWM (SVPWM) scheme. In [11] and [12], a modified virtual-space-vector (VSV)-based modulation method is put forward for the diode-clamped three-level converter applied in an aircraft ESG prototype system, which achieves NP voltage balance and common-mode voltage (CMV) reduction. It is worth noting that the suppression of NP voltage ripple and NP potential balancing

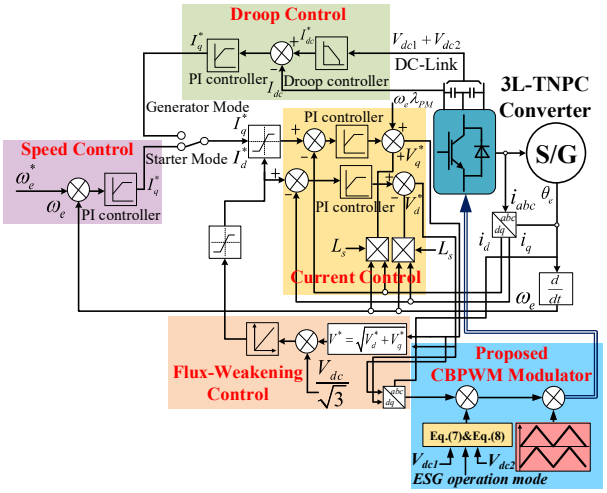

Fig. 3: Control blocks of the studied ESG system.

are achieved at the cost of additional switching actions. To overcome unnecessary switching actions in the starter mode, a hybrid VSV modulation algorithm is presented in the works of [13]. In addition, VSV-based PWM has been explored to boost dc-link voltage utilization for the NPC topology [14], [15]. The latter is the carrier-based PWM (CBPWM) strategy that is preferable for multilevel converters due to its simplicity and easy implementation. The author in [16] proposed a method by injecting an optimized zero-sequence voltage (ZSV). In [17], an advanced discontinuous PWM (DPWM) method has been proposed by injecting two different types of ZSV, but the injected signal needs to be divided so as to avoid abrupt commutation. Research on a flexible DPWM has been carried out for traction drives featuring a seamless shift from sinusoidal PWM (SPWM) to DPWM scheme [18]. In [19] and [20], the g-h coordinate-based SVPWM and CBPWM are investigated to implement VSVs, respectively, aiming to keep two capacitor voltages balanced. However, the thermal issue stands out during the entire operating points of the drives.

In this paper, according to the operation status of the target ESG system, a versatile CBPWM strategy is proposed through a flexible ZSV injection. During the startup process, a proper ZSV is selected to fulfill the commutation requirement. When the motor speed approaches 20 krpm, a smooth shift for obtaining a lower switching loss is enabled, which is beneficial for heavy-duty operation in the power generating mode. In addition, with the NP potential bias feedback control, the deviated NP voltage is balanced again.

II. The Existing CBPWM Strategy for T-type Three-Level Converter

Fig.2 presents the circuit diagram of the 3L-TNPC converter. As can be seen, each phase consists of four switches (S_{x1}~S_{x4}), in which phase x denotes phase-A, B or C. Two identical capacitors (C_1 and C_2) are series-connected to form the DC-link. Three-phase modulation references V_{ma}, V_{mb} and V_{mc} and output phase currents i_a, i_b and i_c can be expressed as follows:

$$\begin{cases} V_{ma} = m\cos(\omega t) \\ V_{mb} = m\cos(\omega t - 2\pi/3) \\ V_{mc} = m\cos(\omega t + 2\pi/3) \end{cases} \tag{1}$$

$$\begin{cases} i_a = I_o\cos(\omega t - \varphi) \\ i_b = I_o\cos(\omega t - \varphi - 2\pi/3) \\ i_c = I_o\cos(\omega t - \varphi + 2\pi/3) \end{cases} \tag{2}$$

where V_{ma}, V_{mb} and V_{mc} are normalized with respected to the half of the DC-link voltage, m indicates the modulation index and ω is angular frequency. I_o denotes the amplitude of phase current and φ represents the power factor angle.

When a phase terminal is clamped to the midpoint of DC-link, the phase current charges or discharges NP potential, thus shifting capacitor voltages. The average NP current over a carrier period can be calculated by:

$$\overline{i_{NP}} = d_{ao}\cdot i_a + d_{bo}\cdot i_b + d_{co}\cdot i_c \tag{3}$$

where d_{ao}, d_{bo} and d_{co} are the phase duty cycle that generate zero-level voltage.

Besides, the duty cycle of phase-x clamping to positive/negative of DC-rail and the NP should meet the constraint in each carrier period: d_{xp}+d_{xo}+d_{xn}=1, where d_{xo} is given in (4) based on the volts-second principle:

$$d_{xo} = 1 - |V_{mx}| \tag{4}$$

Substituting (1) and (4) into (3) yields the expression of NP current:

$$\overline{i_{NP}} = \sum_{i=a,b,c}(1 - |V_{mi}|)\cdot i_i \tag{5}$$

As a result, the capacitor voltage variation over a switching period, i.e., T_s, can be derived as:

$$V_{NP} = \frac{1}{C}\int_0^{T_s}\overline{i_{NP}}\cdot dt \tag{6}$$

Thus, NP potential is influenced by the current flowing into or out of the NP. Noted that the ac component of (6) denotes NP voltage ripple and DC component of (6) causes a static error between two capacitor voltages. Also, the frequency of this ripple is three times of fundamental frequency.

III. Proposed CBPWM Strategy for the ESG System Operating in a Wide-Speed Range

A. NP current analysis for a flexible zero-sequence voltage injection

Compared with the commonly-used zero-sequence component $V_{off} = -0.5(V_{\max} + V_{\min})$, the generalized ZSV offset can be expressed as:

$$V_{gen.off} = k\cdot(1 - V_{\max}) + (1-k)\cdot(-1 - V_{\min}) \tag{7}$$

where V_{max} and V_{min} are the maximum and minimum value of three-phase reference voltages produced by the inner current loop, respectively. k is a coefficient that can be tuned for generating a series of zero-sequence components. $V_{gen.off}$ is defined as a positive-type 3^{rd}-order harmonic component in

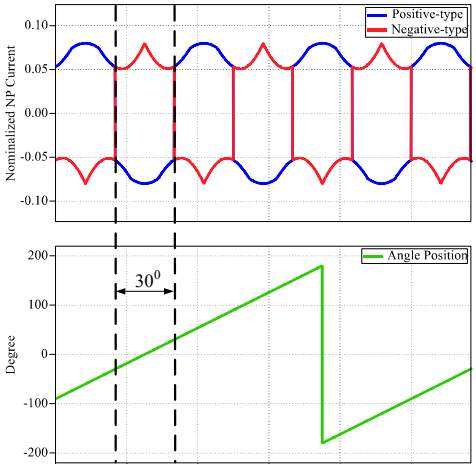

(a)

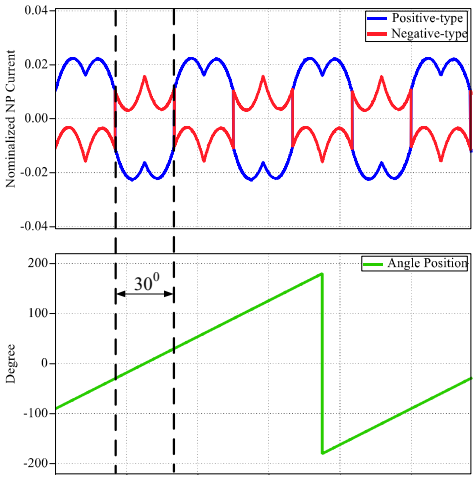

(b)

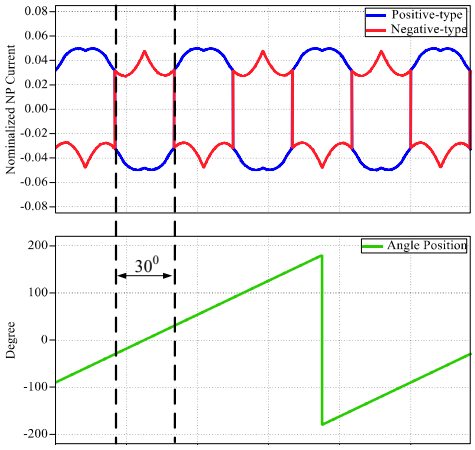

(c)

Fig. 4: Normalized NP current and angle position. (m=0.8 and PF=1) (a) k=0.6. (b) k=0.7. (c) k=0.8.

the paper. Similarly, another zero-sequence voltage defined as negative counterpart can be given by:

$$V_{gen.off}^{'} = (1-k)\cdot(1-V_{\max}) + k\cdot(-1-V_{\min}) \qquad (8)$$

As mentioned above, NP voltage drift can be controlled by manipulating NP current over a carrier period. NP currents

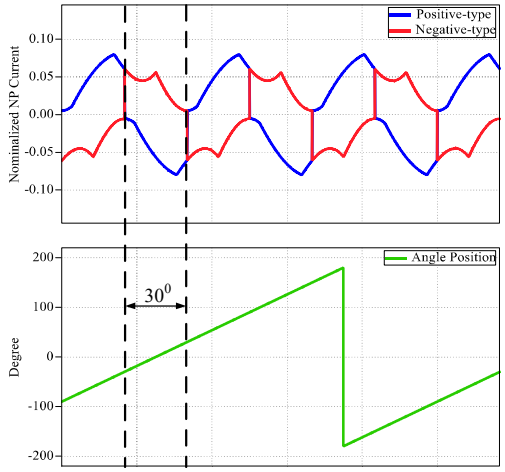

(a)

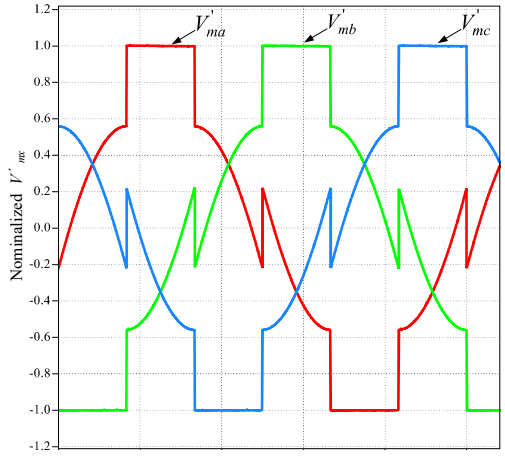

(b)

Fig. 5: k equals 1. (m=0.9 and PF=0.86) (a) Normalized NP current and angle position. (b) Three-phase modulation waveforms.

produced by positive/negative-type ZSVs are hence analyzed and calculated by (5). In addition, the corresponding angle position of approximated reference voltage vector is detected. The normalized NP current and the angle position, when k equals 0.6, 0.7 and 0.8 (MI=0.8 and PF =1), are depicted in Fig.4. As can be observed, the pulsation of NP current is periodically alternating between positive and negative in every 30°. Thus, the desired NP current associated with favorable polarity can be used to correct NP voltage imbalance.

When modulation index ramps up to 0.9 and power factor drops to 0.86, k raises to 1 for gaining maximum NP voltage control capability in generation mode. The normalized NP currents with corresponding angle position is shown in Fig.5(a). Each modulation waveform injected by zero-sequence component, as shown in Fig.5(b), is alternatively clamped in every 60°. This means the presented strategy is able to transit to 60°-clamped DPWM, thereby reducing switching actions.

The proposed three-level CBPWM strategy are summarized as follows: two capacitor voltages are detected and compared over a carrier period. When V_{dc1} is larger than V_{dc2}, (7) or (8) generating positive NP current is chosen in every 30°; when V_{dc1} is smaller than V_{dc2}, negative NP current offered by (7)

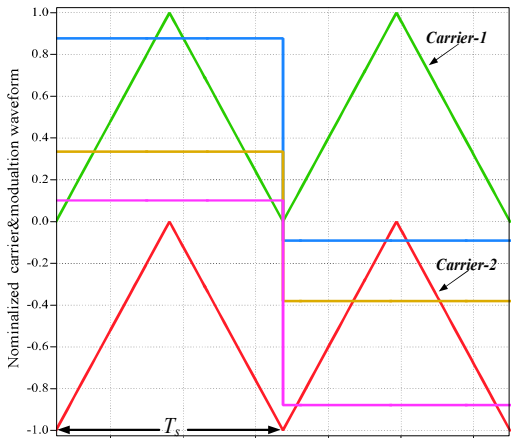

(a)

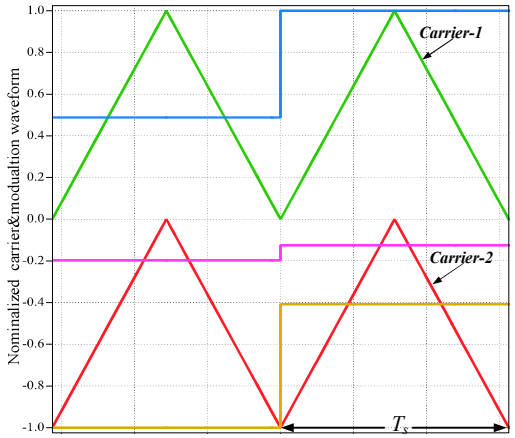

(b)

Fig. 6: Nominalized carrier/modulation signals. (a) k=0.9 and m=0.4. (b) k=1 and m=0.9.

TABLE I: ESG system parameters

Parameters	Value
L_d = L_q	99 μH
Pole pair	3
Base speed	8 krpm
Switching frequency	50 kHz
PM flux	0.03644 V_s/rad
Fundamental frequency	$\leq$ 1 kHz
Capacitor value (C_1=C_2)	600 μF
DC-link voltage	540 V

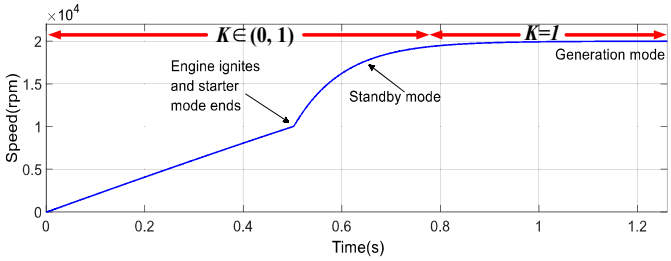

Fig. 7: PMSM speed diagram at every stage.

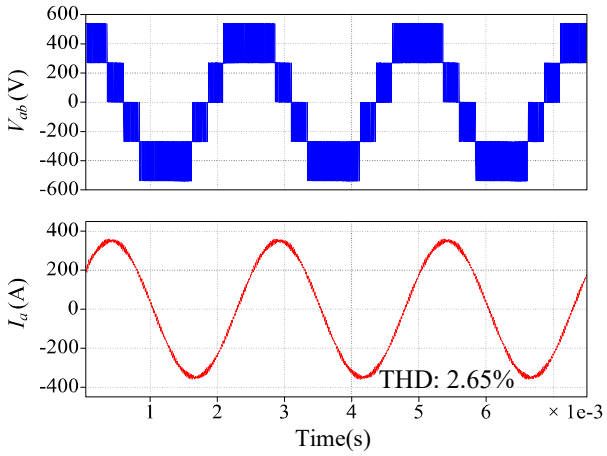

(a)

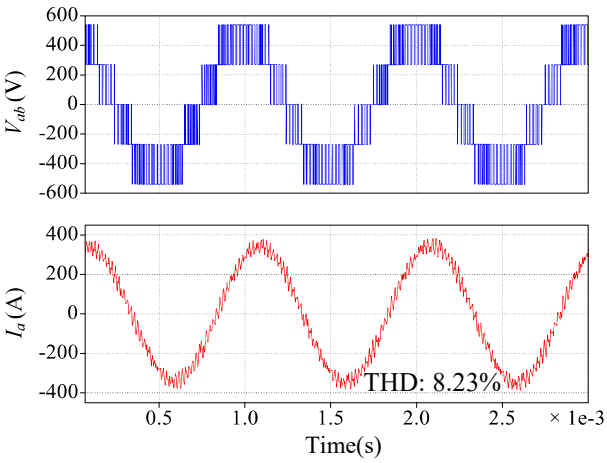

(b)

Fig. 8: Phase current and line-to-line voltage at a PMSM speed of (a) 8 krpm and (b) 20 krpm.

or (8) is selected in every 30°. With the feedback control, the NP voltage balance can be maintained. In terms of switching action, the presented scheme allows k to be flexibly tuned without breaking the rules of commutation, as shown in Fig.6. In contrast to the method discussed in [17], this characteristic is another advantage of the presented technique.

IV. Simulation and Experimental Results

The designed 200 kW, ±270 VDC bipolar aircraft ESG system using a SiC-based 3L-TNPC converter is built in the MATLAB/PLECS environment. The system parameters are detailed in Table 1. CAS480M12HM3 power module is chosen to analyze power losses. In the startup process, k is a flexible coefficient that is larger than 0 but less than 1. When the machine speed is over 20 krpm, the generation mode is activated. At that time, k raises up to 1 for mitigating switching actions. In Fig.7, the speed diagram describes the ESG system status at every stage. The phase current and line-to-line voltage at 8 krpm and 20 krpm are shown in Fig.8. NP voltage balancing performance under a fundamental frequency of 1 kHz is shown in Fig.9, where k equals 0.8 and 20 V bias initially exists between two capacitors. Fig.10 shows the total loss map among the conventional DPWM, 3^{rd}-order harmonic injected SPWM and the proposed CBPWM when the target system

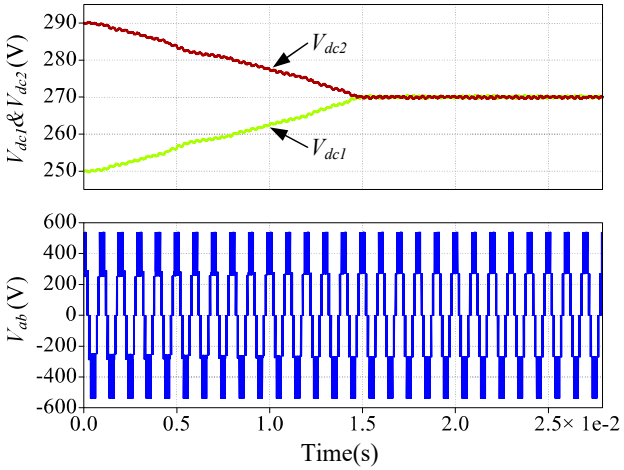

Fig. 9: V_{dc1}, V_{dc2} and line-to-line voltage (k=0.8).

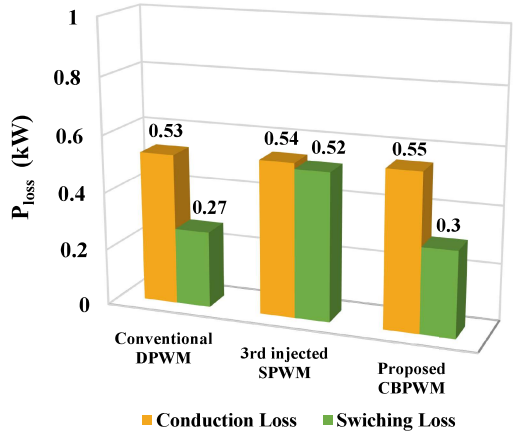

Fig. 10: Power loss breakdown (k=1).

delivers 75% rated power in generation mode. As shown, the proposed CBPWM strategy significantly reduces switching loss compared with the 3^{rd}-harmonic injected SPWM while maintaining a similar power loss map compared with the conventional DPWM method. Fig.11 presents the designed SiC-based 3L-TNPC platform for future experimental tests. At the initial stage of the laboratory development, the proposed modulation strategy is tested at a fundamental frequency of 1 kHz and k=0.8 under a modulation index of 0.9 and a load factor of 0.8. Fig.12 shows an existing NP voltage deviation of 30 V is quickly kept balanced again within 6.27 ms.

V. Conclusion

In this paper, a new CBPWM algorithm with a flexible ZSV injection method is proposed for a 3L-TNPC converter used in the high-speed aerospace drives. In accordance with the operation mode of target drive systems, the multi-ZSV components are dynamically chosen. Not only can the strategy correct NP potential drift, but also it brings a chance to lower switching loss. Additionally, the undesirable commutation is avoided effectively. The simulation and experimental results successfully demonstrate the good performance of the proposed modulation technique for the SiC-based three-level power generation unit in the ESG system of the MEA.

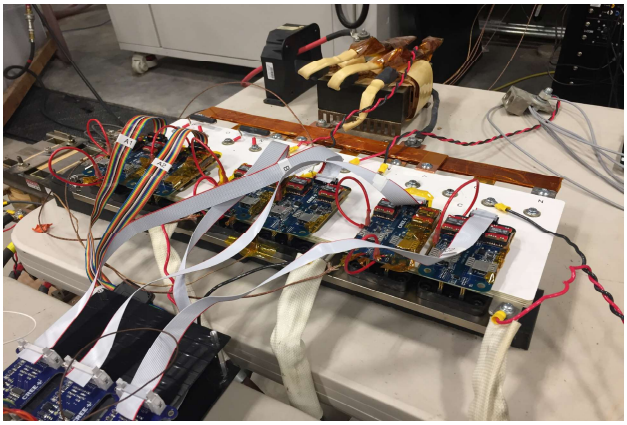

Fig. 11: SiC-based 3L-TNPC test bench.

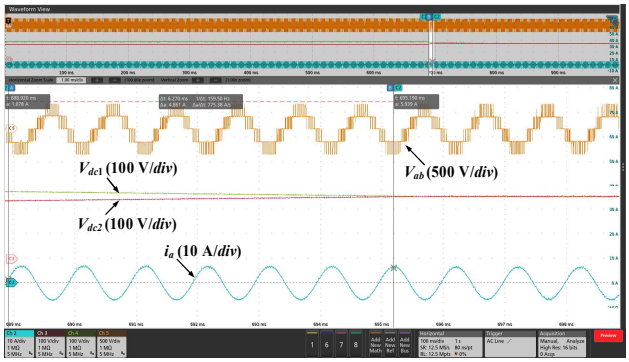

Fig. 12: Capacitor voltage recovery process when k=0.8 at a fundamental frequency of 1 kHz.

References

[1] P. Wheeler, T. S. Sirimanna, S. Bozhko and K. S. Haran, "Electric/hybrid-electric aircraft propulsion systems," *Proc. IEEE.*, vol. 109, no. 6, pp. 1115-1127, Jun. 2021.

[2] Y. Chen, L. Du and J. He, "Online diagnosis and ride-through operation for cascaded H-bridge converter based STATCOM with a single open-circuit IGBT," *IEEE Trans. Ind. Electron.*, vol. 69, no. 8, pp. 7549-7559, Aug. 2022.

[3] F. Diao, G. Zhu, Y. Wu, Y. Li, Z. Ma and Y. Zhao, "A modular and performance-tunable silicon carbide half-bridge building block with digital gate driver," *2022 IEEE Applied Power Electronics Conference and Exposition (APEC)*, Houston, TX, USA, 2022, pp. 251-258.

[4] L. Du and J. He, "A simple autonomous phase-shifting PWM approach for series-connected multi-converter harmonic mitigation," *IEEE Trans. Power Electron.*, vol. 34, no. 12, pp. 11516-11520, Dec. 2019.

[5] X. Lyu, H. Li, Z. Ma, B. Hu and J. Wang, "Dynamic voltage balancing for the high-voltage SiC super-cascode power switch," *IEEE J. Emerg. Sel. Topics Power Electron.*, vol. 7, no. 3, pp. 1566-1573, Sept. 2019.

[6] J. He, L. Du, S. Yuan, C. Zhang and C. Wang, "Supply voltage and grid current harmonics compensation using multi-port interfacing converter integrated into two-ac-bus grid," *IEEE Trans. Smart Grid.*, vol. 10, no. 3, pp. 3057-3070, May 2019.

[7] J. Zeng, X. Du and Z. Yang, "A multiport bidirectional DC–DC converter for hybrid renewable energy system integration," *IEEE Trans. Power Electron.*, vol. 36, no. 11, pp. 12281-12291, Nov. 2021.

[8] F. Diao, G. Zhu, A. Rockhill, H. Cao, Y. Wu and Y. Zhao, "Physics-based magnetic modeling of a three-port transformer in a triple-active-bridge converter with decoupled power flow regulation," *2022 IEEE Applied Power Electronics Conference and Exposition (APEC)*, Houston, TX, USA, 2022, pp. 1492-1499.

[9] H. Cao, G. Zhu, F. Diao and Y. Zhao, "Novel power decoupling methods for three-port triple-active-bridge converters," *2022 IEEE Applied Power Electronics Conference and Exposition (APEC)*, Houston, TX, USA, 2022, pp. 1833-1837.

[10] Z. Wang, Y. Wu, M. H. Mahmud, Z. Zhao, Y. Zhao, and H. A. Mantooth, "Design and validation of a 250-kW all-silicon carbide high-density three-level T-type inverter," *IEEE J. Emerg. Sel. Topics Power Electron.*, vol. 8, no. 1, pp. 578-588, Mar. 2020.

[11] Z. Zeng, X. Zhang, F. Blaabjerg, H. Chen and T. Sun, "Stepwise design methodology and heterogeneous integration routine of air-cooled SiC inverter for electric vehicle," *IEEE Trans. Power Electron*., vol. 35, no. 4, pp. 3973-3988, Apr. 2020.

[12] H. Chen *et al*., "Design and optimization of SiC MOSFET wire bondless power modules," *2020 IEEE 9th international power electronics and motion control conference (IPEMC2020-ECCE Asia)*, Nanjing, China, 2020, pp. 725-728.

[13] F. Guo, T. Yang, S. Bozhko and P. Wheeler, "A novel virtual space vector modulation scheme for three-level NPC power converter with neutral-point voltage balancing and common-mode voltage reduction for electric starter/generator system in more-electric-aircraft," in *Proc. IEEE Energy Convers. Congrs. Expo.*, pp. 1852-1858, Sep. 2019.

[14] F. Guo, T. Yang, A. M. Diab, S. S. Yeoh, S. Bozhko, and P. Wheeler, "An enhanced virtual space vector modulation scheme of three-level NPC converters for more-electric-aircraft applications," *IEEE Trans. Ind. Appl.*, vol. 57, no. 5, pp. 5239-5251, Sept.-Oct. 2021.

[15] F. Guo *et al*., "Hybrid active modulation strategy for three-level neutral-point-clamped converters in high-speed aerospace drives," *IEEE Trans. Ind. Electron.*, doi: 10.1109/TIE.2022.3176309

[16] S. Busquets-Monge, R. Maheshwari and S. Munk-Nielsen, "Overmodulation of *n*-level three-leg DC-AC diode-clamped converters with comprehensive capacitor voltage balance," *IEEE Trans. Ind. Electron*., vol. 60, no. 5, pp. 1872-1883, May 2013.

[17] F. Guo *et al.*, "An overmodulation algorithm with neutral-point voltage balancing for three-level converters in high-speed aerospace drives," *IEEE Trans. Power Electron*., vol. 60, no. 5, pp. 1872-1883, May 2013.

[18] C. Wang and Y. Li, "Analysis and calculation of zero-sequence voltage considering neutral-point potential balancing in three-level NPC converters," *IEEE Trans. Ind. Electron.*, vol. 57, no. 7, pp. 2262-2271, Jul. 2010.

[19] J. Lee, S. Yoo and K. Lee, "Novel discontinuous PWM Method of a three-Level inverter for neutral-point voltage ripple reduction," *IEEE Trans. Ind. Electron*, vol. 63, no. 6, pp. 3344-3354, Jun. 2016.

[20] S. Mukherjee, S. K. Giri, and S. Banerjee, "A flexible discontinuous modulation scheme with hybrid capacitor voltage balancing strategy for three-level NPC traction inverter," *IEEE Trans. Ind. Electron*, vol. 66, no. 5, pp. 3333-3343, May 2019.

[21] F. Guo, T. Yang, S. Bozhko and P. Wheeler, "3L-NPC AC-DC power converter using virtual space vector PWM with optimal switching sequence based on g-h coordinate," *2018 IEEE International Conference on Electrical Systems for Aircraft, Railway, Ship Propulsion and Road Vehicles & International Transportation Electrification Conference (ESARS-ITEC),* Nottingham, UK, 2018, pp. 1-7.

[22] F. Guo, T. Yang, C. Li, S. Bozhko and P. Wheeler, "Active modulation strategy for capacitor voltage balancing of three-level neutral-point-clamped converters in high-speed drives," *IEEE Trans. Ind. Electron.*, vol. 69, no. 3, pp. 2276-2287, Mar. 2022.